OPEN ACCESS
Journal of Innovative Optical Health Sciences
Vol. 16, No. 4 (2023) 2243005 (13 pages)

DOI: 10.1142/S1793545822430052

World Scientific
www.worldscientific.com

Three-dimensional remodeling of collagen fibers within cervical tissues in pregnancy

Lingxi Zhou*,‖, Rushan Jiang*,‖, Jia Meng*, Shuhao Qian*, Shenyi Jiang*, Chuncheng Wang*, Chen Yang*, Zhihua Ding*, Zheyue Shu‡,§ and Zhiyi Liu*,†,¶

*State Key Laboratory of Modern Optical Instrumentation
College of Optical Science and Engineering
International Research Center for Advanced Photonics
Zhejiang University, Hangzhou, Zhejiang 310027, P. R. China

†Intelligent Optics & Photonics Research Center
Jiaxing Research Institute, Zhejiang University
Jiaxing, Zhejiang 314000, P. R. China

‡Division of Hepatobiliary and Pancreatic Surgery
Department of Surgery, The First Affiliated Hospital
Zhejiang University School of Medicine
Hangzhou, Zhejiang 310027 P. R. China
§shuzheyue@zju.edu.cn
¶liuzhiyi07@zju.edu.cn

Received 29 July 2022
Revised 5 December 2022
Accepted 6 December 2022
Published 18 January 2023

The cervix is a collagen-rich connective tissue that must remain closed during pregnancy while undergoing progressive remodeling in preparation for delivery, which begins before the onset of the preterm labor process. Therefore, it is important to resolve the changes of collagen fibers during cervical remodeling for the prevention of preterm labor. Herein, we assessed the spatial organization of collagen fibers in a three-dimensional (3D) context within cervical tissues of mice on day 3, 9, 12, 15 and 18 of gestation. We found that the 3D directional variance, a novel metric of alignment, was higher on day 9 than that on day 3 and then gradually decreased from day 9 to day 18. Compared with two-dimensional (2D) approach, a higher sensitivity was achieved from 3D analysis, highlighting the importance of truly 3D quantification. Moreover, the depth-dependent variation of 3D directional variance was investigated. By combining multiple 3D directional variance-derived metrics, a high level of classification accuracy was acquired in distinguishing different periods of pregnancy. These results demonstrate that 3D directional

§,¶Corresponding authors.
‖Lingxi Zhou and Rushan Jiang contributed equally to this paper.

variance is sensitive to remodeling of collagen fibers within cervical tissues, shedding new light on highly-sensitive, early detection of preterm birth (PTB).

Keywords: Preterm birth; cervical tissue; directional variance; collagen fiber; 3D analysis.

1. Introduction

Preterm birth (PTB) is most commonly defined as birth before 37 weeks of gestation for human beings.[1] Complications associated with PTB, the leading cause of neonatal mortality and the largest contributor to under-five mortality globally, affect 10.6% of pregnant women worldwide, equal to an estimated 14.84 million births.[2] These complications include intraventricular hemorrhage (IVH), respiratory distress syndrome (RDS), retinopathy of prematurity (ROP), cerebral palsy, necrotizing enteritis, sepsis, chronic lung disease, neonatal infection and patent ductus arteriosis.[3,4] Therefore, it is of great clinical significance to take effective and safe measures for the detection and prevention of PTB. Previous studies have shown that abnormal or inappropriately-timed cervical remodeling can lead to PTB.[5] Cervix is a collagen-rich connective tissue, which must remain closed during pregnancy, and at the same time, undergo a progressive remodeling for birth preparation.[6] It is an active, dynamic process when cervix transforms from a closed rigid structure to a sufficiently open one, which begins long before the onset of labor.[7] Cervical remodeling can be divided into four distinct but overlapping phases termed softening, ripening, dilation and postpartum repair.[8,9] The fact that the cervix is mainly connective tissue, predominately collagen, was first reported in 1947.[10] Leppert demonstrated that fibrillar collagen was the main structural protein that influenced the tensile properties of the cervix.[11] In addition, recent studies confirmed that changes in collagen structure preceded cervical softening and contributed to the progressive decline in the tensile strength of the cervix. Therefore, morphological and organizational changes of collagen fibers can potentially serve as a sensitive biomarker for monitoring cervical remodeling in gestation.[12]

In biological tissues, collagen fibers have strong second-order nonlinear polarizability and noncentrosymmetric structure, which can generate strong second harmonic generation (SHG) signals,[13,14] with advantages of little photo-damage and photo-toxicity. SHG has emerged as a powerful tool for imaging collagen fibers of different biological tissues with sub-micrometer resolution in a completely label-free manner.[15–19] However, even as high-resolution three-dimensional (3D) images of collagen fibers become more readily accessible, quantitative analysis methodologies for their orientation and organization have largely remained limited to analysis of two-dimensional (2D) images,[12,20,21] with a few notable exceptions only.[22–24]

To establish the real architecture of collagen fibers in biological tissues, we developed a 3D orientation determination algorithm which provided voxel-wise orientation information with high accuracy, and offered advantages in computational time and sensitivity over previous approaches.[25] Based on the 3D orientation, we further proposed a novel optical metric termed 3D directional variance which was able to provide a direct, simplified estimation of spatial organization of collagen fibers in a truly 3D context.[26] This metric ranges between 0 and 1, with 0 corresponding to perfectly parallel alignment of fibrillar structures, while 1 corresponding to complete randomness.[26] Using this metric, we have recognized specific characteristics of collagen fibers in a variety of diseases including breast cancer, pancreatic cancer, ovarian cancer, peritoneal metastasis and arthritis,[26–29] as well as in engineered tissues where cell-matrix interactions in response to different treatments are investigated.[30–32]

In this study, label-free SHG images of collagen fibers are acquired from cervical tissues of mice on day 3, 9, 12, 15 and 18 during the 19-day mouse gestation, and the 3D orientation and directional variance assessments are applied to the analysis of these collagen fiber images. A comparison of 2D and 3D analysis is performed. By exploring the collagen fiber organization in a truly 3D way, we obtain information of dynamic cervical remodeling in gestation of mouse model, highlighting the potential of the quantitative SHG imaging in staging pregnancy.

2. Materials and Methods

2.1. *Cervical tissue preparation*

Mice were housed together at $\sim 24^{\circ}$C, relative humidity of 55–65% with a 12 h light/dark cycle and fed with standard chow and water. On days 3, 9, 12, 15 and 18 of gestation, mice were sacrificed and cervical tissues were harvested. Fresh tissues were used for imaging immediately following excision. We cut tissues with a size of approximately $3 \times 3 \times 1.5$ mm, at the location close to the side of external os in the cervix [marked by the green box in Fig. 1(a)], and the orientation of the cutting plane was perpendicular to the inner canal. All the experimental procedures for mice were approved by the Animal Use and Care Committee at Zhejiang University and in accordance with the National Institutes of Health Guidelines.

2.2. *SHG image acquisition*

The schematic of the imaging system is shown in Fig. 1(a). SHG and two-photon excited fluorescence (TPEF) images (512×512 pixels; $386 \times 386\,\mu$m) were collected from a custom-built multiphoton microscope. Laser emission from a mode-locked Ti: sapphire laser (Spectra Physics, MaiTai) was focused by a water-immersion 25× objective (NA 0.95; 2.4 mm working distance) for the excitation of harmonophores and endogenous fluorophores (such as nicotinamide adenine dinucleotide, NAD(P)H and flavin adenine dinucleotide, FAD, data not shown) at 800 nm with average laser power of 40 mW. SHG and fluorescence signals were collected through the same objective and spectrally separated by a sequence of dichroic mirrors and filters. Optical signals were detected by a pair of GaAsP photomultiplier tubes (PMT), each behind a bandpass filter for isolating SHG (400 ± 10 nm) or fluorescence (460 ± 20 nm) signals. In this study, the gain was kept the same for the two PMTs and throughout all the experiments; therefore, the image intensity was calculated and normalized by the square of the incident laser power, as measured at the sample plane prior to each experiment. As shown in Fig. 1(a), the imaging area was right close

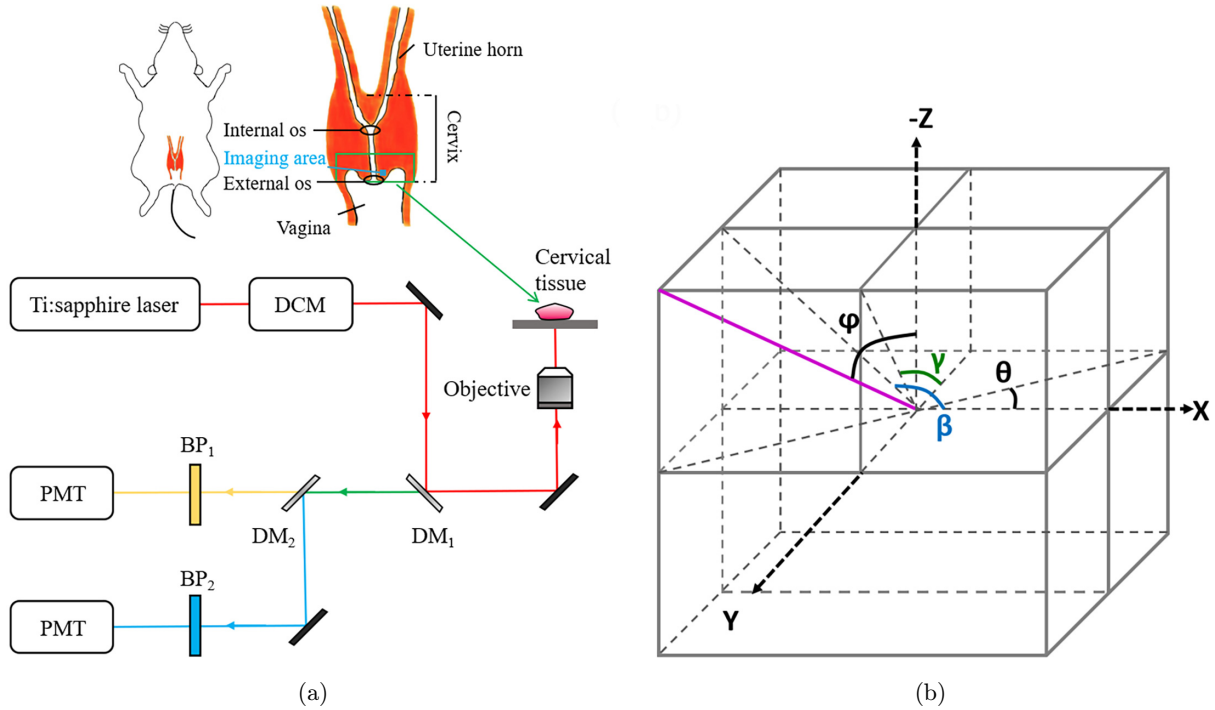

Fig. 1. Schematic of the sample preparation, imaging system and analysis algorithm to extract the 3D alignment of fiber-like structures. (a) Illustration of the location of the harvested tissues and the imaging area, as well as the layout of the imaging system. BP, bandpass tunable filter; DCM, dispersion compensation module; DM, dichroic mirror; PMT, photomultiplier tube. (b) Definition of angles to depict a certain orientation (the magenta line) in 3D space. (c) Validation of the analysis algorithm by comparing the directional variance maps (middle row) and corresponding distributions (bottom row) of simulated 3D fiber stacks (top row) with gradients in alignment level (fibers being more disorganized from left to right).

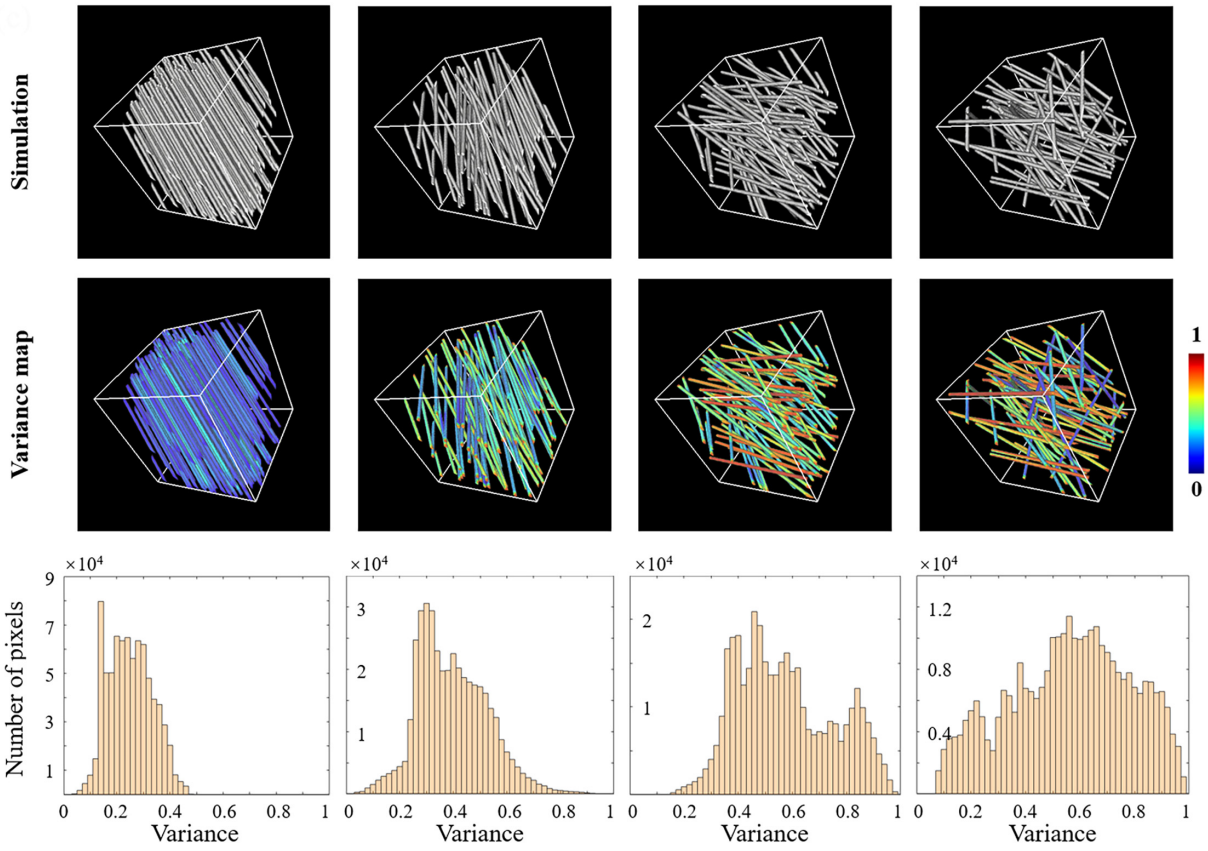

(c)

Fig. 1. (*Continued*)

to the inner canal and selected beneath the squamous epithelium, approximately 100 μm from the surface. Cervical tissues were acquired from 4 mice at each time point (day 3, 9, 12, 15 and 18) of gestation, with one or two tissue specimens harvested from each mouse, leading to totally six tissue specimens at each time point. Two SHG 3D image stacks, recorded 2 μm apart, were acquired from each tissue specimen for data analysis.

2.3. *3D analysis of orientation and organization*

In 2D space, the spatial orientation of a fiber could be described by the azimuthal angle θ. While in 3D space, both azimuthal angle θ and polar angle φ were needed to depict a certain orientation [Fig. 1(b)]. Actually, it was not straightforward to calculate the polar angle φ. To address this issue, we defined another two azimuthal angles, β and γ, which were related to the polar angle φ with the following equation[25]:

$$\tan^2\varphi = 1/\tan^2\beta + 1/\tan^2\gamma, \tag{1}$$

where γ is defined as the angle between the fiber's projection in the yz plane and the $-y$ axis, and β is defined as the angle between the fiber's projection in the zx plane and the x axis [Fig. 1(b)]. In our previous study, we developed the weighted vector summation algorithm for the determination of θ, β and γ, thus obtaining the orientation information of any fiber direction in 3D space.[25]

Based on the 3D orientation information, we further proposed a novel optical metric termed 3D directional variance, V_{3D}, which provided a simple but highly-accurate measure of fiber-like structures in a 3D context,[26] with its definition shown as follows:

$$V_{3D} = 1 - \bar{R}_{3D}, \tag{2}$$

$$\bar{R}_{3D} = (\bar{C}_{3D}^{\,2} + \bar{S}_{3D}^{\,2} + \bar{Z}_{3D}^{\,2})^{1/2}. \tag{3}$$

Besides, we defined $b_j = \sqrt{1/\tan^2(2\beta_j) + 1/\tan^2(2\gamma_j)}$ to derive these components as follows:

$$\bar{C}^{\,a}_{3D} = (1/n)\sum_{j=1}^{n}(b_j/\sqrt{1+b_j^2})\cos(2\theta_j), \quad (4)$$

$$\bar{S}^{\,a}_{3D} = (1/n)\sum_{j=1}^{n}(b_j/\sqrt{1+b_j^2})\sin(2\theta_j), \quad (5)$$

$$\bar{Z}^{\,a}_{3D} = (1/n)\sum_{j=1}^{n}\mathrm{SI}/\sqrt{1+b_j^2}, \quad (6)$$

where $\mathrm{SI} = (-1)\cdot(\varphi - 90)/|\varphi - 90|$ when $\varphi \neq 90°$, and $\mathrm{SI} = 1$ when $\varphi = 90°$. Here n indicates the total number of voxels devoted to the calculation of 3D directional variance. As mentioned above, 3D directional variance ranged between 0 and 1, with a lower variance value corresponding to a more parallel alignment.[26]

To demonstrate the ability of the 3D algorithm in describing the orientation and organization of fiber-like structures, we simulated four stacks with a size of $200 \times 200 \times 200$ voxels containing fibers with gradients in alignment, which became more and more disorganized (corresponding to a higher directional variance level) from left to right [Fig. 1(c), top]. Then, the 3D analysis algorithm was applied to those stacks to obtain 3D directional variance maps [Fig. 1(c), middle], along with corresponding distribution histograms [Fig. 1(c), bottom]. As expected, fibers with a better alignment led to a lower peak location in variance distribution histograms, and *vice versa*. These results proved that the 3D directional variance in this study was a simple while highly-sensitive metric that accurately described the organization of fiber-like structures in a 3D context.

2.4. *Statistical analysis*

For statistical analysis, a one-way ANOVA with *post-hoc* Tukey HSD test was used to assess significant differences using JMP. Results are considered significant at $p < 0.05$. To verify the ability of the 3D directional variance related metrics in distinguishing different periods of gestation, we performed canonical linear discriminant analysis using SPSS, and original classification accuracy (OCA) and cross-validated classification accuracy (CVCA) were acquired, respectively, based on the entire dataset and the leave-one-out cross validation dataset.

3. Results and Discussion

3.1. *Overview of 3D fiber alignment at different periods of gestation*

First of all, we tried to gain an overview of the 3D orientation and organization of collagen fibers in cervical tissues of pregnant mice at different periods, i.e., day 3, 9, 12, 15 and 18 of the 19-day mouse gestation. Representative SHG images of collagen fibers from distinct gestational days are shown in Fig. 2(a). The cervical remodeling in pregnancy most likely occurred at length-scales ranging from the molecule to the tissue level (∼10 nm–10 mm), i.e., from the collagen fibrils (∼10–500 nm) gathering together to form collagen fibers (∼1–500 μm) and the collagen fibers further bundling together to form the tissue level ultrastructure (∼1–10 mm).[33] Owing to the spatial resolution of SHG microscopy, we focused on and quantified the micrometer-scale organization of collagen fibers within pregnant mouse cervix. By performing our 3D orientation algorithm on 3D collagen fiber image stacks from these specific periods, we obtained corresponding θ [Fig. 2(b)] and φ [Fig. 2(c)] orientation maps. Note that representative maps at the same tissue depth were shown here. As can be seen from θ orientation maps [Fig. 2(b)], collagen fibers on day 3 exhibited relatively uniform hues, indicating that these fibers oriented consistently along a certain direction, in contrast to variations in hues observed from the θ map on day 9. However, φ orientation maps from all the periods [Fig. 2(c)] typically exhibited greenish hues (corresponding to φ orientation of $\sim 90°$), although heterogeneity in hues on each map was observed, revealing that collagen fibers mainly aligned parallel to the optical sections (i.e., the plane of these 2D frames).

Then, we acquired the 3D directional variance maps at these periods accordingly [Fig. 2(d)], along with corresponding distribution histograms [Fig. 2(e)] of all the collagen fibers on these representative frames. As revealed by blue hues of the variance map on day 3, there was a low level of variance at the beginning of pregnancy, indicating that at this stage, collagen fibers aligned orderly. In contrast, collagen fibers were found to exhibit a high level of variance on day 9, corresponding to a rather random alignment at the middle of gestation. Interestingly, hues of the variance maps on day 12, 15 and 18 were at an intermediate status, indicating that collagen fibers might undergo remodeling

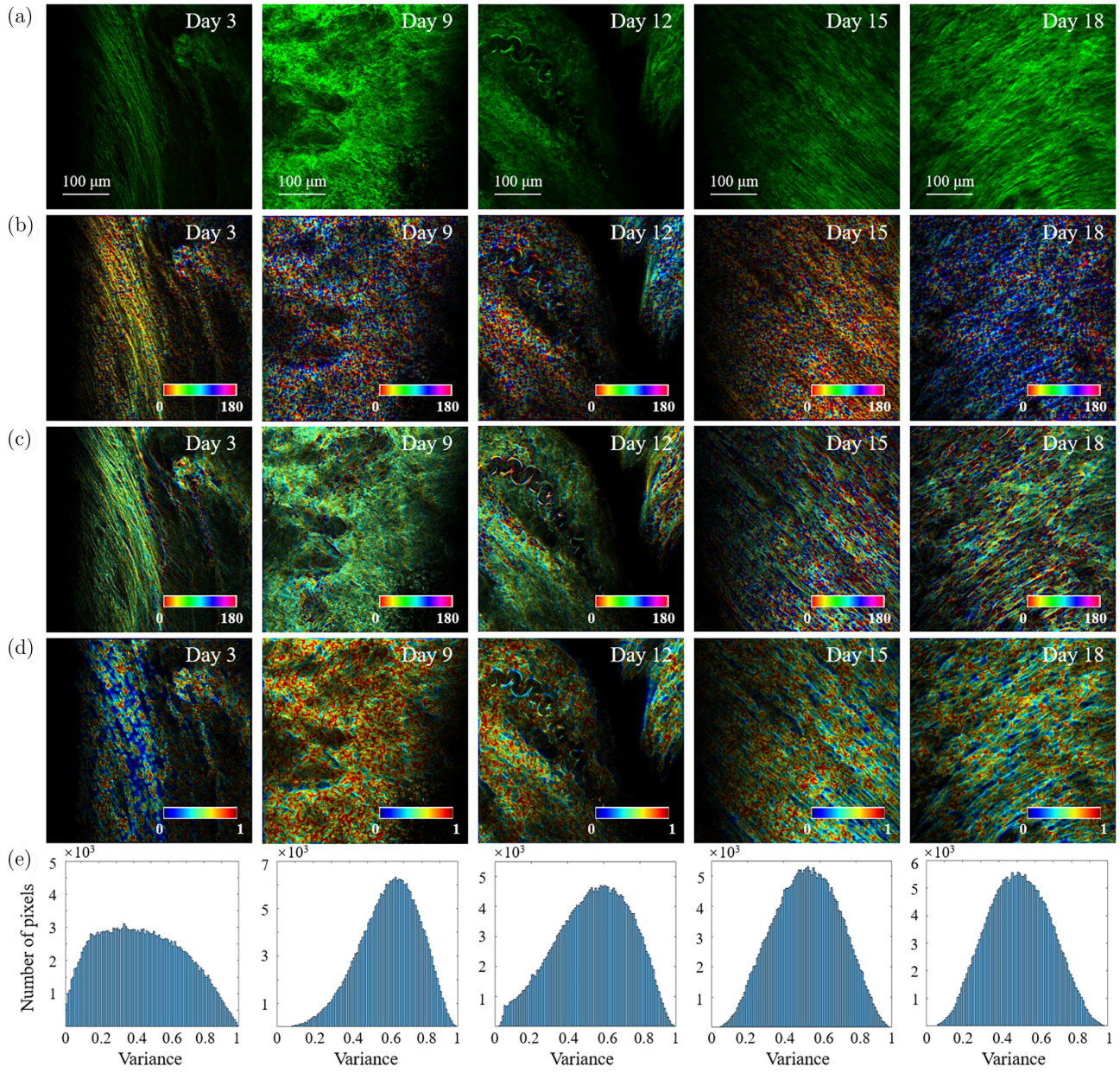

Fig. 2. Representative images and corresponding maps of tissue samples acquired from different periods of gestation. (a) SHG images from day 3, 9, 12, 15 and 18 of gestation. (b) Color-coded θ orientation maps. (c) Color-coded φ orientation maps. (d) 3D directional variance maps. (e) 3D directional variance distributions.

following the trend of a better alignment at relatively late gestation stage, although the exact date of re-aligning needed to be investigated in more detail. These observations from 3D directional variance maps were consistent with the distribution histograms [Fig. 2(e)], where the distribution peak was centered at a low variance level on day 3 (i.e., around 0.3 in this case), while at a high level on day 9 (i.e., around 0.65) and a level in-between on day 12, 15 and 18 (i.e., around 0.5–0.6).

3.2. *Comparison of 3D and 2D analyses*

These observations of differences in color-coded 3D directional variance maps [Fig. 2(d)] or variance distributions [Fig. 2(e)] acquired by 3D algorithm [Fig. 3(a), top], were further validated by statistical analysis [Fig. 3(a), bottom]. The mean directional variance increased from day 3 to day 9, and then gradually decreased from day 9 to day 18, with significance levels labeled in the plot. In order to

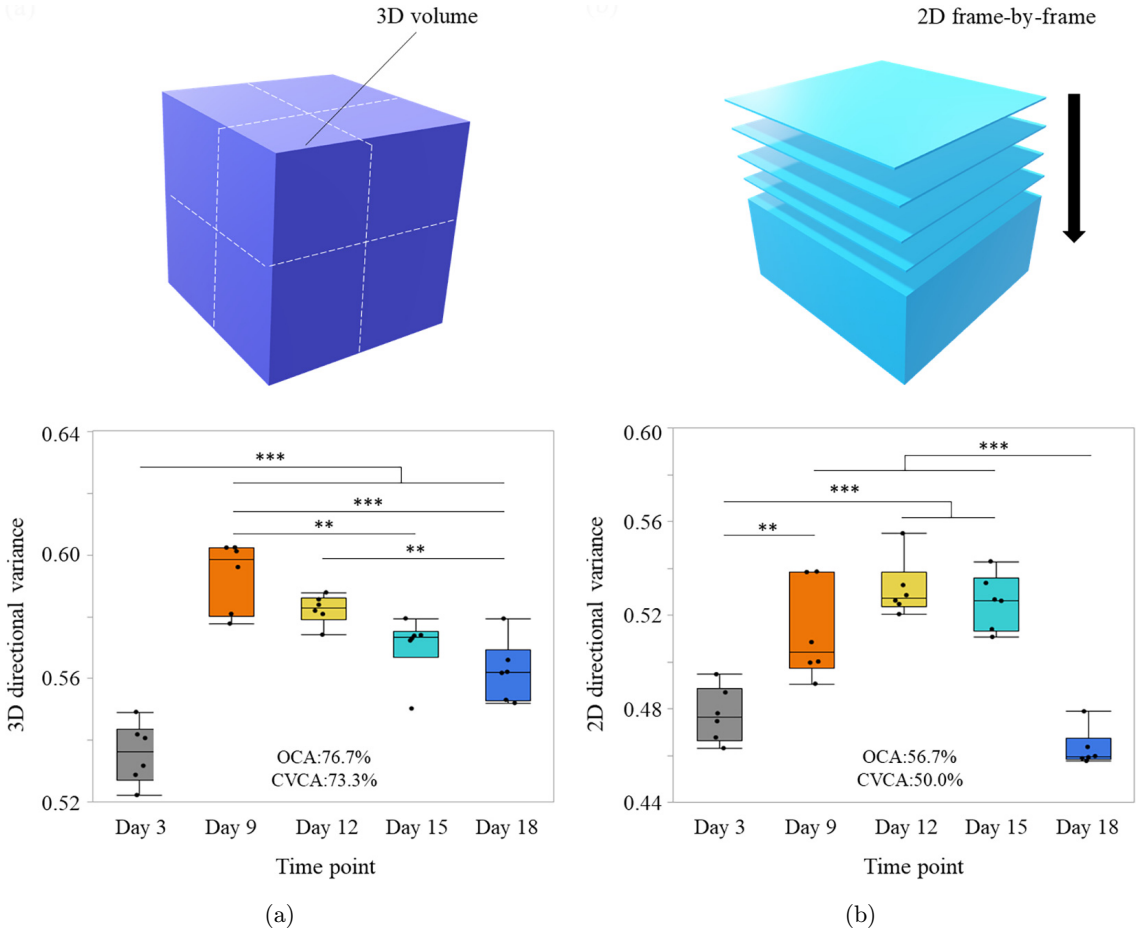

Fig. 3. Comparison of 3D and 2D analysis. (a) 3D analysis scheme (top) and boxplot of 3D analysis results at different time points (bottom). (b) 2D analysis scheme (top) and boxplot of 2D analysis results at different time points (bottom). $n = 6$ tissues at each time point. **, $p < 0.01$; ***, $p < 0.001$.

demonstrate the sensitivity enhancement achieved by employing a 3D image analysis approach for the acquired 3D stacks, we compared the results with that from a typical 2D image analysis method. As shown in the schematic [Fig. 3(b), top], this approach was based on estimating the 2D directional variance frame-by-frame,[30] and analysis results were obtained accordingly [Fig. 3(b), bottom]. Besides, we calculated OCA and CVCA to reveal the ability of staging gestation by 3D and 2D variance analysis (see Methods), with these values shown in each boxplot. Although 2D analysis led to similar trends in directional variance as 3D analysis, the classification accuracy values were different. Specifically, 3D analysis led to 76.7% in OCA and 73.3% in CVCA, in contrast to 56.7% in OCA and 50.0% in CVCA by 2D analysis. Such a comparison revealed that 3D analysis was more sensitive in identifying organizational differences in 3D stacks of collagen fiber images than 2D image-based method, which was sensitive to changes in θ orientation only.

3.3. *Depth-dependent features of 3D fiber alignment*

To take advantage of 3D nature of the image stack, we assessed the depth-dependent profiles of directional variance. Specifically, we applied the 3D directional variance algorithm to the 3D image stacks of cervical specimens from representative time points, i.e., day 3, 9 and 18 of gestation [Fig. 4(a)], and acquired the directional variance maps at different depths, with six representative ones shown in Fig. 4(b). Then, we plotted and fitted the mean variance of each frame as a function of depth [Fig. 4(c)]. As can be seen from these profiles, collagen fibers from different periods of gestation exhibited different features in the average level and fluctuation of

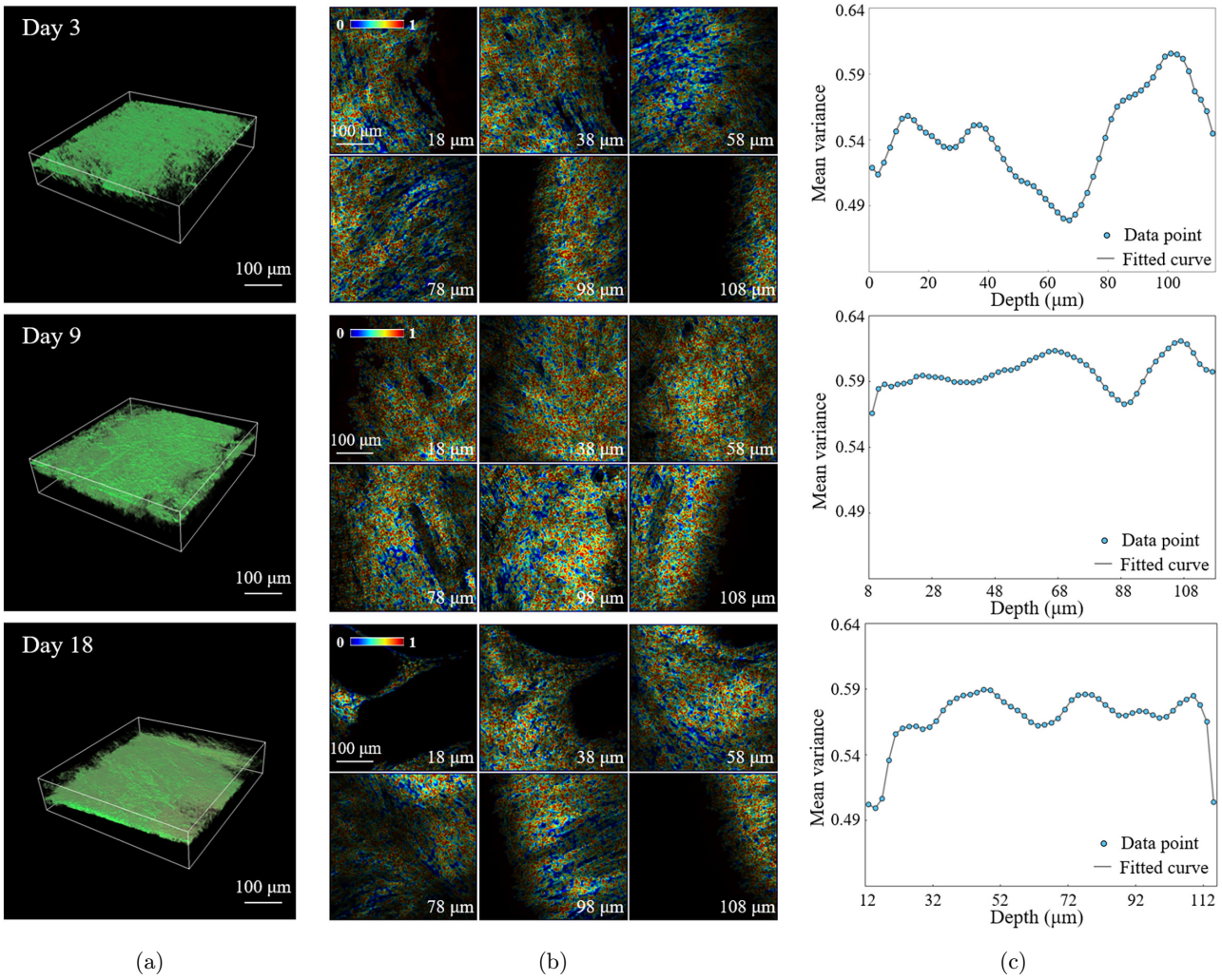

Fig. 4. Directional variance changes with depth following different profiles at different periods of gestation. (a) 3D reconstruction of collagen fiber images of cervical tissue specimens from representative time points, i.e., day 3, day 9 and day 18 of gestation. (b) Directional variance maps at six representative depths. (c) Depth-dependent 3D directional variance profiles.

variance. Generally, collagen fibers from day 9 specimens exhibited a high level of directional variance, in contrast to that from day 3 and day 18 specimens. Moreover, we observed a relatively higher fluctuation in depth-dependent profiles of directional variance from day 3 and day 18 specimens contrasted to day 9 ones, indicating that the variation in variance throughout imaging depth might potentially serve as an optical biomarker for staging gestation.

3.4. *Staging mice gestation using 3D directional variance related measures*

Inspired by the observations mentioned above, we generated the standard deviation of mean variance with depth (MVWD) to represent the depth-dependent variation, and assessed its ability in staging gestation. This metric was able to distinguish certain time points, and we obtained an OCA of 53.5% and a CVCA 40.0% in classifying all the groups [Fig. 5(a)]. Besides, in complement to standard deviation, we acquired the range of the depth-dependent dataset, as calculated from the difference between the maximum and the minimum variance value along the depth. Similarly, this metric led to an OCA of 56.7% and a CVCA 53.3% [Fig. 5(b)]. Finally, we investigated the informational complementarity from these 3D directional variance-derived measures, i.e., the mean variance, and standard deviation and range of MVWD, in understanding and identification of specific gestation

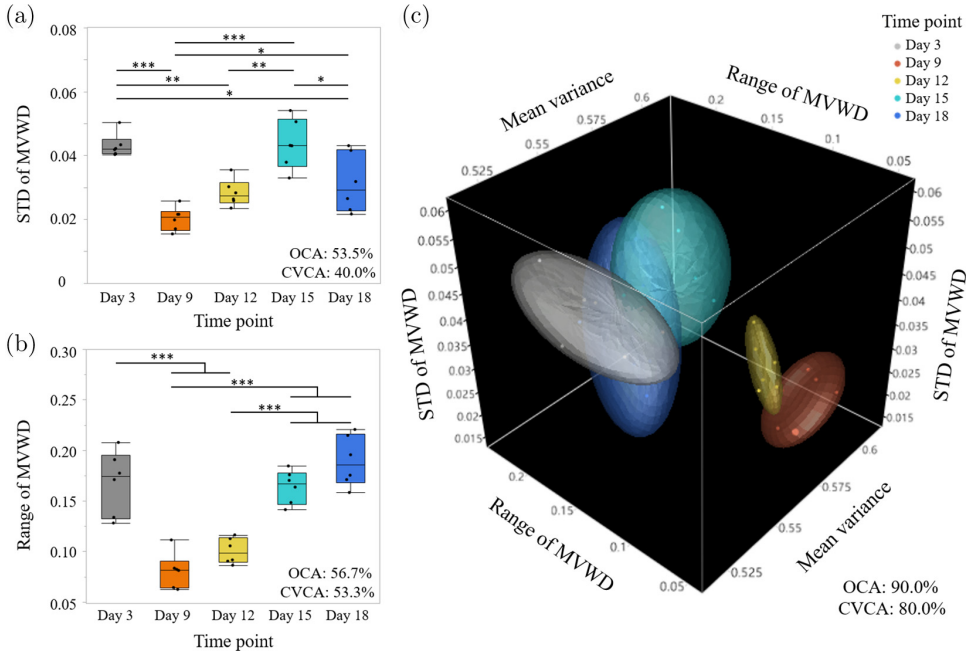

Fig. 5. Classification of different groups using different optical metrics or a combination of them. (a) Boxplot of standard deviation of MVWD at different time points. (b) Boxplot of range of MVWD at different time points. (c) 3D scatterplot showing the classification of cervical tissues at different periods in pregnancy using a combination of three directional variance-related optical metrics. STD: standard deviation. OCA and CVCA values are marked in each panel. $n = 6$ tissues at each time point. $^{*}p < 0.05$; $^{**}p < 0.01$; $^{***}p < 0.001$.

periods. Owing to the powerful classification capability by combining insights from different aspects, an OCA of 90.0% and a CVCA of 80.0% were achieved [Fig. 5(c)], highlighting the potential of multi-parametric analysis.

3.5. *Discussion*

In this study, we employed the 3D directional variance analysis to resolve the potential cervical remodeling in mouse gestation, in a completely automated and quantitative manner, with collagen fiber images that were acquired label-free from SHG imaging. Although SHG provided the ability of 3D imaging, previous studies focused on collagen orientation or organization readouts mainly based on analysis of 2D images;[34] in contrast, the 3D directional variance offered a truly 3D assessment of collagen fiber organization with enhanced sensitivity, as validated from the 3D versus 2D comparison in this study. A possible reason was that 3D analysis stacked up collagen fibers without discarding potential direction information (i.e., the φ orientation in this context),[30] which might more faithfully represent the actual spatial organization of fibrillar structures in 3D space.

The 3D directional variance analysis enabled us to gain a better understanding of the collagen fiber organization at distinct periods of gestation, which drew lots of attention in recent years and became a target of PTB researches. Akins *et al.* used SHG microscopy to assess changes in collagen structure of murine cervix during cervical remodeling of pregnancy by collecting both forward and backward SHG signals, and found that the fiber size progressively increased from early to late pregnancy, while pores between collagen fibers became larger and farther apart.[35] With home-built SHG scanning endomicroscope, Zhang *et al.* found that the diameter of collagen fibers and the fractional area and mean gray value (MGV) of the collagen signals would gradually increase in mouse gestation, and qualitative impression of a degradation in collagen fiber alignment with progression of gestation was acquired.[5] Using the quantitative 3D SHG microscopy, Moghaddam *et al.* assessed the collagen fiber alignment at distinct regions of the internal os side in rat cervix, including the outer zone, the inner zone and the septum, and demonstrated that rat cervical remodeling during pregnancy was not uniform across the cervix.[36] Especially, they found that the alignment of collagen fibers in the inner zone

increased with the gestational day from the nonpregnant cervix to day 15 but then progressively decreased from day 15 to day 21, which could only be resolved from the 3D analysis, instead of the 2D analysis.[36] Similarly, in our study, we also found that the alignment of collagen fibers was not changing unidirectionally throughout the entire progress of mice gestation, as revealed by our highly-sensitive 3D directional variance analysis. Specifically, collagen fibers on day 9 were significantly less aligned than that on day 3, while fibers on day 18 were more aligned than that on day 9. These subtle changes could hardly be obtained from traditional qualitative observations, highlighting the sensitivity of the quantitative 3D analysis, although the underlying mechanisms for the observed collagen reprogramming was worthy for future investigations. Interestingly, Yoshida *et al.* reported that the immature crosslink density followed the similar trends as the directional variance level that we observed throughout the mice gestation, as measured from the ultra-performance liquid chromatography-electrospray ionization tandem mass spectrometry.[37] Previous studies found that an increased crosslink density level corresponded to a decrease in collagen fiber organization (i.e., an increase in directional variance) within mice cartilage specimens by immunostaining;[38] thus, the crosslink characterizations by Yoshida *et al.* supported changes in fiber alignment in mice gestation from our study.

We quantified the changes of collagen fiber alignment, as represented by 3D directional variance, in cervical tissues of mice during normal pregnancy, and found that this metric was indeed different at distinct stages of pregnancy, which proved it to be one of the optical biomarkers for collagen structural organization. However, as can be seen from statistical analysis results and classification accuracies, there was still room to improve the staging capability based on collagen fiber signatures. In addition to directional variance, there were several other features closely associated with collagen fiber morphology and organization, including waviness,[27,39] thickness[40] and local density,[28] which might potentially contribute to proper staging of pregnancy. Besides, owing to the ability of this system to acquire TPEF and SHG signals simultaneously (see *Methods*), endogenous fluorescence from coenzymes, such as NAD(P)H and FAD, could be harvested and processed to gain information of cellular metabolism.[41–43] Therefore, the fusion analysis of multiple parameters,[44] from both collagen fibers and cells, would be the goal of our next move to gain a better understanding of collagen arrangement in pregnancy.

Lots of previous studies focused on the mechanical properties of cervix in pregnancy. The most common loading protocol used to measure mechanical properties of rodent cervix was a load-to-break test, where the tissue was continuously displaced until it broke.[45] Despite the variations among studies, load-to-break studies on mouse cervix generally reported that the instantaneous stiffness from nonpregnant to term (day 18) decreased by $\sim$ 20-fold.[45] Interestingly, several studies also observed that the change of stiffness was not unidirectional, with an increase until 6–10 days followed by a decrease after then.[46–48] Even though a more detailed assessment is needed to correlate the tissue stiffness with the directional variance readout reported in this study, other factors such as the collagen content and morphological features might contribute to tissue mechanical properties as well.[18]

There are some limitations in our study. First, we perform *ex vivo* imaging of cervical tissues; therefore, we are not able to assess the collagen fiber remodeling continuously from the same mouse and the analysis results might suffer from artifacts originating from individual differences, which could potentially bring uncertainty to our results. Second, we mainly focus on locations close to the side of external os in cervix. Actually, locations close to the side of the internal os are worthy of future investigations since these locations might provide complementary, region-dependent (including the outer zone, the inner zone and the septum) insights regarding the collagen remodeling.

4. Conclusions

In this study, we apply the quantitative SHG imaging to the assessments of cervical remodeling during normal pregnancy in mouse model. Especially, the 3D directional variance measures enable automated, quantitative, highly-sensitive characterizations of collagen fibers in a truly 3D manner at different periods of gestation. Owing to the sensitivity enhancement by the analysis methodology, we find that the reprogramming of collagen fibers is

not unidirectional. Although in this study, experiments are conducted *ex vivo* using excised tissue specimens, recent developments of probe-based multiphoton microscopes may enable translation of such studies *in vivo* which will offer a unique potential to monitor cervical alterations in normal pregnancy, allow early prediction of PTB risk and facilitate development of therapies for prevention.

Conflict of Interest

The authors declare no conflicts of interest.

Acknowledgments

We thank Prof. Chen-Yuan Dong at National Taiwan University for insightful discussion. This work was supported by the National Natural Science Foundation of China (61905214, 62035011, 11974310 and 31927801), National Key Research and Development Program of China (2019YFE0113700 and 2017YFA0700501) and Natural Science Foundation of Zhejiang Province (LR20F050001). Lingxi Zhou and Rushan Jiang contributed equally to this work.

References

1. L. Liu, S. Oza, D. Hogan, J. Perin, I. Rudan, J. E. Lawn, S. Cousens, C. Mathers, R. E. Black, "Global, regional, and national causes of child mortality: An updated systematic analysis for 2010 with time trends since 2000," *Lancet* **379**, 2151–2161 (2012).
2. S. Chawanpaiboon, J. P. Vogel, A. B. Moller, P. Lumbiganon, M. Petzold, D. Hogan, S. Landoulsi, N. Jampathong, K. Kongwattanakul, M. Laopaiboon, C. Lewis, S. Rattanakanokchai, D. N. Teng, J. Thinkhamrop, K. Watananirun, J. Zhang, W. Zhou, A. M. Gülmezoglu, "Global, regional, and national estimates of levels of preterm birth in 2014: A systematic review and modelling analysis," *Lancet Glob. Health* **7**, E37–E46 (2019).
3. R. M. Ward, J. C. Beachy, "Neonatal complications following preterm birth," *BJOG* **110**, 8–16 (2003).
4. M. J. Platt, "Outcomes in preterm infants," *Public Health* **128**, 399–403 (2014).
5. Y. Y. Zhang, M. L. Akins, K. Murari, J. Xi, M. J. Li, L. P. Katherine, M. Mahendroo, X. Li, "A compact fiber-optic SHG scanning endomicroscope and its application to visualize cervical remodeling during pregnancy," *Proc. Natl. Acad. Sci. USA* **109**, 12878–12883 (2012).
6. Y. Akgul, R. Holt, M. Mummert, A. Word, M. Mahendroo, "Dynamic changes in cervical glycosaminoglycan composition during normal pregnancy and preterm birth," *Endocrinology* **153**, 3493–3503 (2012).
7. B. Timmons, M. Akins, M. Mahendroo, "Cervical remodeling during pregnancy and parturition," *Trends Endocrinol. Metab.* **21**, 353–361 (2010).
8. C. P. Read, R. A. Word, M. A. Ruscheinsky, B. C. Timmons, M. S. Mahendroo, "Cervical remodeling during pregnancy and parturition: Molecular characterization of the softening phase in mice," *Reproduction* **134**, 327–340 (2007).
9. R. A. Word, X. H. Li, M. Hnat, K. Carrick, "Dynamics of cervical remodeling during pregnancy and parturition: Mechanisms and current concepts," *Semin. Reprod. Med.* **25**, 69–79 (2007).
10. D. N. Danforth, "The fibrous nature of the human cervix, and its relation to the isthmic segment in gravid and nongravid uteri," *Am. J. Obstet. Gynecol.* **53**, 541–560 (1947).
11. P. C. Leppert, "Anatomy and physiology of cervical ripening," *Clin. Obstet. Gynecol.* **38**, 267–279 (1995).
12. C. Bayan, J. M. Levitt, E. Miller, D. Kaplan, I. Georgakoudi, "Fully automated, quantitative, noninvasive assessment of collagen fiber content and organization in thick collagen gels," *J. Appl. Phys.* **105**, 102042 (2009).
13. P. J. Campagnola, L. M. Loew, "Second-harmonic imaging microscopy for visualizing biomolecular arrays in cells, tissues and organisms," *Nat. Biotechnol.* **21**, 1356–1360 (2003).
14. J. Li, M. N. Wilson, A. J. Bower, M. Marjanovic, E. J. Chaney, R. Barkalifa, S. A. Boppart, "Video-rate multimodal multiphoton imaging and three-dimensional characterization of cellular dynamics in wounded skin," *J. Innov. Opt. Heal. Sci.* **13**, 2050007 (2020).
15. R. M. Williams, W. R. Zipfel, W. W. Webb, "Interpreting second-harmonic generation images of collagen I fibrils," *Biophys. J.* **88**, 1377–1386 (2005).
16. P. J. Campagnola, A. C. Millard, M. Terasaki, P. E. Hoppe, C. J. Malone, W. A. Mohler, "Three-dimensional high-resolution second-harmonic generation imaging of endogenous structural proteins in biological tissues," *Biophys. J.* **82**, 493–508 (2002).
17. R. Cicchi, N. Vogler, D. Kapsokalyvas, B. Dietzek, J. Popp, F. S. Pavone, "From molecular structure to tissue architecture: Collagen organization probed by SHG microscopy," *J. Biophotonics* **6**, 129–142 (2013).
18. K. P. Quinn, K. E. Sullivan, Z. Liu, Z. Ballard, C. Siokatas, I. Georgakoudi, L. D. Black, "Optical

metrics of the extracellular matrix predict compositional and mechanical changes after myocardial infarction," *Sci. Rep.* **6**, 35823 (2016).
19. L. Qiu, D. Kang, C. Wang, W. Guo, F. Fu, Q. Wu, G. Xi, J. He, L. Zheng, Q. Zhang, X. Liao, L. Li, J. Chen, H. Tu, "Intratumor graph neural network recovers hidden prognostic value of multi-biomarker spatial heterogeneity," *Nat. Commun.* **13**, 4250 (2022).
20. E. Brown, T. McKee, E. diTomaso, A. Pluen, B. Seed, Y. Boucher, R. K. Jain, "Dynamic imaging of collagen and its modulation in tumors in vivo using second-harmonic generation," *Nat. Med.* **9**, 796–800 (2003).
21. K. P. Quinn, A. Golberg, G. F. Broelsch, S. Khan, M. Villiger, B. Bouma, W. G. Austen Jr., R. L. Sheridan, M. C. Mihm Jr., M. L. Yarmush, I. Georgakoudi, "An automated image processing method to quantify collagen fibre organization within cutaneous scar tissue," *Exp. Dermatol.* **24**, 78–80 (2015).
22. A. J. Schriefl, G. Zeindlinger, D. M. Pierce, P. Regitnig, G. A. Holzapfel, "Determination of the layer-specific distributed collagen fibre orientations in human thoracic and abdominal aortas and common iliac arteries," *J. R. Soc. Interface* **9**, 1275–1286 (2012).
23. T. Y. Lau, R. Ambekar, K. C. Toussaint, "Quantification of collagen fiber organization using three-dimensional Fourier transform-second-harmonic generation imaging," *Opt. Exp.* **20**, 21821–21832 (2012).
24. H. Altendorf, E. Decencière, D. Jeulin, P. D. E. S. A. Peixoto, A. Deniset-Besseau, E. Angelini, G. Mosser, M. Schanne-Klein, "Imaging and 3D morphological analysis of collagen fibrils," *J. Microsc.* **247**, 161–175 (2012).
25. Z. Y. Liu, K. P. Quinn, L. Speroni, L. Arendt, C. Kuperwasser, C. Sonnenschein, A. M. Soto, I. Georgakoudi, "Rapid three-dimensional quantification of voxel-wise collagen fiber orientation," *Biomed. Opt. Exp.* **6**, 2294–2310 (2015).
26. Z. Y. Liu, D. Pouli, D. Sood, A. Sundarakrishnan, C. K. H. Mingalone, L. M. Arendt, C. Alonzo, K. P. Quinn, C. Kuperwasser, L. Zeng, T. Schnelldorfer, D. L. Kaplan, I. Georgakoudi, "Automated quantification of three-dimensional organization of fiber-like structures in biological tissues," *Biomaterials* **116**, 34–47 (2016).
27. S. H. Qian, J. Meng, Z. Feng, L. X. Zhou, S. Y. Jiang, Y. L. Wang, Z. T. Ye, S. M. Zhuo, J. X. Chen, X. J. Li, L. X. Gao, Z. H. Ding, J. Qian, Z. Y. Liu, "Mapping organizational changes of fiber-like structures in disease progression by multi-parametric, quantitative imaging," *Laser Photon. Rev.* **16**, 2100576 (2022).
28. S. H. Qian, G. X. Wang, J. Meng, S. Y. Jiang, L. X. Zhou, J. P. Lu, Z. H. Ding, S. M. Zhuo, Z. Y. Liu, "Identification of human ovarian cancer relying on collagen fiber coverage features by quantitative second harmonic generation imaging," *Opt. Exp.* **30**, 25718–25733 (2022).
29. C. K. H. Mingalone, Z. Y. Liu, J. M. Hollander, K. D. Garvey, A. L. Gibson, R. E. Banks, M. Zhang, T. E. McAlindon, H. C. Nielsen, I. Georgakoudi, L. Zeng, "Bioluminescence and second harmonic generation imaging reveal dynamic changes in the inflammatory and collagen landscape in early osteoarthritis," *Lab. Invest.* **98**, 656–669 (2018).
30. Z. Liu, L. Speronib, K. P. Quinn, C. Alonzo, D. Pouli, Y. Zhang, E. Stuntz, C. Sonnenschein, A. M. Soto, I. Georgakoudi, "3D organizational mapping of collagen fibers elucidates matrix remodeling in a hormone-sensitive 3D breast tissue model," *Biomaterials* **179**, 96–108 (2018).
31. A. Sundarakrishnan, H. Zukas, J. Coburn, B. T. Bertini, Z. Y. Liu, I. Georgakoudi, L. Baugh, Q. Dasgupta, L. D. Black, D. L. Kaplan, "Bioengineered in vitro tissue model of fibroblast activation for modeling pulmonary fibrosis," *ACS Biomater. Sci. Eng.* **5**, 2417–2429 (2019).
32. M. Q. Huang, G. S. Cai, L. M. Baugh, Z. Y. Liu, A. Smith, M. Watson, D. Popovich, T. Y. Zhang, L. S. Stawski, M. Trojanowska, I. Georgakoudi, L. D. BlackIII, P. A. Pioli, M. L. Whitfield, J. Garlick, "Systemic sclerosis dermal fibroblasts induce cutaneous fibrosis through lysyl oxidase-like 4: New evidence from three-dimensional skin-like tissues," *Arthritis Rheumatol.* **72**, 791–801 (2020).
33. K. M. Myers, H. Feltovich, E. Mazza, J. Vink, M. Bajka, R. J. Wapner, T. J. Hall, M. House, "The mechanical role of the cervix in pregnancy," *J. Biomech.* **48**, 1511–1523 (2015).
34. G. Q. Xi, L. D. Qiu, S. Y. Xu, W. H. Guo, F. M. Fu, D. Y. Kang, L. Q. Zheng, J. J. He, Q. Y. Zhang, L. H. Li, C. Wang, J. X. Chen, "Computer-assisted quantification of tumor-associated collagen signatures to improve the prognosis prediction of breast cancer," *BMC Med.* **19**, 273 (2021).
35. M. L. Akins, K. Luby-Phelps, M. Mahendroo, "Second harmonic generation imaging as a potential tool for staging pregnancy and predicting preterm birth," *J. Biomed. Opt.* **15**, 026020 (2010).
36. A. O. Moghaddam, Z. Lin, M. Sivaguru, H. Phillips, B. L. McFarlin, K. C. Toussaint, A. J. W. Johnson, "Heterogeneous microstructural changes of the cervix influence cervical funneling," *Acta Biomater.* **140**, 434–445 (2022).
37. K. Yoshida, H. F. Jiang, M. J. Kim, J. Vink, S. Cremers, D. Paik, R. Wapner, M. Mahendroo, K. Myers, "Quantitative evaluation of collagen

crosslinks and corresponding tensile mechanical properties in mouse cervical tissue during normal pregnancy," *Plos One* **9**, e112391 (2014).

38. J. H. Kim, G. Lee, Y. Won, M. J. Lee, J. S. Kwak, C. H. Chun, J. S. Chun, "Matrix cross-linking-mediated mechanotransduction promotes posttraumatic osteoarthritis," *Proc. Natl. Acad. Sci. USA* **112**, 9424–9429 (2015).
39. S. H. Qian, J. Meng, W. J. Liu, C. C. Wang, R. S. Jiang, L. Yang, X. Liu, C. F. Kuang, Z. H. Ding, Z. Y. Liu, "Identification of endoplasmic reticulum formation mechanism by multi-parametric, quantitative super-resolution imaging," *Opt. Lett.* **47**, 357–360 (2022).
40. J. Meng, Z. Feng, S. H. Qian, C. C. Wang, X. J. Li, L. X. Gao, Z. H. Ding, J. Qian, Z. Y. Liu, "Mapping physiological and pathological functions of cortical vasculature through aggregation-induced emission nanoprobes assisted quantitative, in vivo NIR-II imaging," *Biomater. Adv.* **136**, 212760 (2022).
41. Z. Y. Liu, D. Pouli, C. A. Alonzo, A. Varone, S. Karaliota, K. P. Quinn, K. Münger, K. P. Karalis, I. Georgakoudi, "Mapping metabolic changes by noninvasive, multiparametric, high-resolution imaging using endogenous contrast," *Sci. Adv.* **4**, eaap9302 (2018).
42. Z. Y. Liu, C. Y. Chiang, J. Nip, L. Feng, Y. Zhang, S. Rocha, I. Georgakoudi, "Nicotinamide effects on the metabolism of human fibroblasts and keratinocytes assessed by quantitative, label-free fluorescence imaging," *Biomed. Opt. Exp.* **12**, 6375–6390 (2021).
43. M. T. Wang, L. Wang, X. M. Zheng, J. Zhou, J. J. Chen, Y. J. Zeng, J. L. Qu, Y. H. Shao, B. Z. Gao, "Nonlinear scanning structured illumination microscopy based on nonsinusoidal modulation," *J. Innov. Opt. Heal. Sci.* **14**, 2142002 (2021).
44. K. Wang, Y. Pan, X. L. Chen, S. Tong, H. P. Liang, Y. Lu, P. Qiu, "3-photon fluorescence and third-harmonic generation imaging of myelin sheaths in mouse digital skin in vivo: A comparative study," *J. Innov. Opt. Heal. Sci.* **15**, 2250003 (2022).
45. K. Yoshida, C. Jayyosi, N. Lee, M. Mahendroo, K. M. Myers, "Mechanics of cervical remodelling: Insights from rodent models of pregnancy," *Interface Focus* **9**, 20190026 (2019).
46. K. Yoshida, M. Mahendroo, J. Vink, R. Wapner, K. Myers, "Material properties of mouse cervical tissue in normal gestation," *Acta Biomater.* **36**, 209 (2016).
47. C. E. Barnum, J. L. Fey, S. N. Weiss, G. Barila, A. G. Brown, B. K. Connizzo, S. S. Shetye, M. A. Elovitz, L. J. Soslowsky, "Tensile mechanical properties and dynamic collagen fiber re-alignment of the murine cervix are dramatically altered throughout pregnancy," *J. Biomech. Eng.-T. Asme* **139**, 0610081–0610087 (2017).
48. S. Nallasamy, K. Yoshida, M. Akins, K. Myers, R. Iozzo, M. Mahendroo, "Steroid hormones are key modulators of tissue mechanical function via regulation of collagen and elastic fibers," *Endocrinology* **158**, 950–962 (2017).